Steady-State Fluorescence and Molecular-Modeling Studies of Tomaymycin–DNA Adducts†

Mary D. Barkley,* T. J. Thomas,‡ and Karol Maskos
Department of Chemistry, Louisiana State University, Baton Rouge, Louisiana 70803
William A. Remers
Department of Medicinal Chemistry, College of Pharmacy, University of Arizona Tucson, Arizona 85721
Received October 4, 1990; Revised Manuscript Received January 25, 1991

ABSTRACT: The interaction of tomaymycin and 8-*O*-methyltomaymycin with calf thymus DNA was studied by steady-state fluorescence techniques. The 8-phenolic proton of tomaymycin has a pK = 8.0, and the phenolate anion is essentially nonfluorescent. However, the fluorescence of the DNA adduct does not decrease until pH >10.5, when the DNA double helix denatures. Acrylamide quenches the fluorescence of the free antibiotic with a quenching rate constant $k_q = 7 \times 10^9$ M^{-1} s^{-1}. In DNA adducts, the quenching rate constant is reduced about 50-fold, indicating that the aromatic ring of the drug is shielded from the solvent. The four possible binding modes of the antibiotics were modeled on a 6-mer duplex by molecular mechanics calculations in the absence and presence of water and counterions. The modeling studies show that the antibiotic is buried in the minor groove in all binding modes, with the 8-substituent pointing away from the DNA core. Three or five waters are displaced from the minor groove, depending on the orientation of the drug on the DNA.

Tomaymycin (Figure 1) and other members of the pyrrolo[1,4]benzodiazepine group of antitumor antibiotics form labile covalent adducts with DNA (Hurley, 1977; Hurley & Needham-VanDevanter, 1986). These drugs bond in the minor groove of the DNA double helix, held by an aminal linkage from C11 of the pyrrolo[1,4]benzodiazepine to N2 of guanine (Graves et al., 1984; Boyd et al., 1990a). The reaction is specific for guanine bases in B-form DNA, but the occupancy of a site as well as the stereochemistry of the linkage and the orientation of the drug in the minor groove vary with pyrrolo[1,4]benzodiazepine structure and flanking base sequence (Graves et al., 1985; Hertzberg et al., 1986; Cheatham et al., 1988; Hurley et al., 1988; Boyd et al., 1990a,b). Presumably the ultimate DNA-reactive species is the N10–C11 imine intermediate shown in Figure 2, which undergoes nucleophilic attack by the exocyclic amino group of guanine (Barkley et al., 1986; Hurley et al., 1988).

Three oligonucleotide duplex adducts of pyrrolo[1,4]-benzodiazepines have been studied by high-field NMR techniques (Graves et al., 1984, 1985; Cheatham et al., 1988; Boyd et al., 1990a,b). The covalent linkage site on the drug was established from the ^{13}C NMR spectrum of [11-^{13}C]-anthramycin bonded to calf thymus DNA fragments (Graves et al., 1984). The covalent linkage site on DNA was conclusively demonstrated in ^1H NMR studies of the bis-tomaymycin–d(CICGAATTCICG)$_2$ adduct (Boyd et al., 1990a). Anthramycin bonds to d(ATGCAT)$_2$ with an 11S stereochemistry and with the aromatic ring to the 3′ side of the covalently modified guanine (Graves et al., 1985; Boyd et al., 1990b), whereas tomaymycin forms both 11S and 11R diastereomeric adducts with the aromatic ring in the 3′ and 5′ orientations, respectively (Cheatham et al., 1988). On the other hand, tomaymycin forms only the 11S adduct with a 3′ orientation on d(CICGAATTCICG)$_2$ (Boyd et al., 1990a). The flexibility of the diazepine ring precludes unambiguous assignment of the stereochemistry of the aminal linkage from NMR data alone. Molecular mechanics calculations were used to predict the structures and relative stabilities of the four possible binding modes for each drug–oligomer adduct (Remers et al., 1986; Cheatham et al., 1988; Boyd et al., 1990a,b). Fluorescence lifetime data for the tomaymycin adducts supported the stereochemical assignments (Cheatham et al., 1988; Boyd et al., 1990a). Close contacts between the concave edge of the pyrrolo[1,4]benzodiazepine and the minor groove of the oligomer duplex were determined from the NOESY[1] spectra of the adducts. For the unique adducts, the solution structure of the oligomer in the presence of bound drug was also studied by NMR (Boyd et al., 1990a,b). Both anthramycin and tomaymycin form relatively nondistortive B-form DNA adducts, with minor perturbations of the sugar–phosphate backbone in the vicinity of the covalent bonding site.

NMR in conjunction with molecular mechanics calculations is a powerful tool for determining the structure of drug–DNA complexes, particularly in cases of multiple binding modes (Cheatham et al., 1988; Boyd et al., 1990a,b; Norman et al., 1990). This approach is capable of providing atomic resolution structural information at the oligonucleotide level. However, optical, hydrodynamic, or chemical methods are necessary to study larger DNA molecules. We have used fluorescence techniques to investigate the interaction of tomaymycin with DNA. This paper reports the spectral characterization of tomaymycin and 8-*O*-methyltomaymycin in solution and bonded to calf thymus DNA. It also presents steady-state

† This work was supported by NIH Grant GM35009.
* Author to whom correspondence should be addressed.
‡ Present address: Division of Rheumatology, Department of Medicine and Clinical Research Center, UMDNJ-Robert Wood Johnson Medical School, New Brunswick, NJ 08903-0019.

[1] Abbreviations: NOESY, two-dimensional nuclear Overhauser effect spectroscopy; TME, tomaymycin 11-methyl ether; TOM, tomaymycin; MTME, 8-*O*-methyltomaymycin 11-methyl ether; MTOM and MTO, 8-*O*-methyltomaymycin; RP-HPLC, reverse-phase high-performance liquid chromatography; EDTA, ethylenediaminetetraacetic acid; P/D, phosphate-to-drug ratio; rms, root-mean-square.

0006-2960/91/0430-4421$02.50/0 © 1991 American Chemical Society

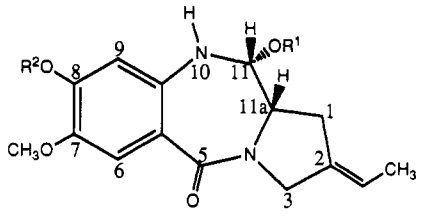

Tomaymycin $R^1=R^2=H$
TME $R^1=CH_3$; $R^2=H$
MTME $R^1=R^2=CH_3$

FIGURE 1: Structures of tomaymycin and related compounds.

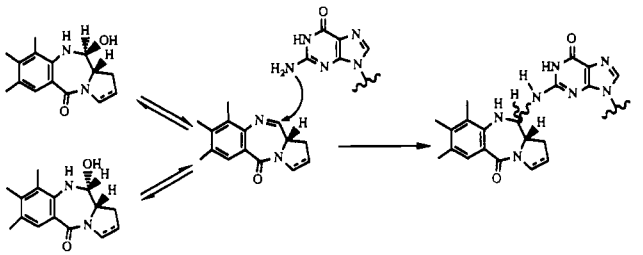

FIGURE 2: Proposed mechanism for the reaction of pyrrolo[1,4]-benzodiazepines with DNA.

fluorescence studies of the drug–DNA adducts. The experimental findings are discussed in light of structural predictions based on molecular mechanics calculations for tomaymycin–oligomer adducts.

Materials and Methods

Chemicals. TME was a generous gift from Dr M. Kohsaka, Fujisawa Pharmaceutical Co. (Japan). MTME was provided by Dr. L. H. Hurley. TME was 98% pure and MTME was 96% pure as determined previously by RP-HPLC (Barkley et al., 1986). Calf thymus DNA (Sigma type I) was purified by phenol extraction and was dialyzed into 0.01 M cacodylate buffer, pH 6.4, or 0.01 M phosphate buffer, pH 7.5, containing 0.1 M NaCl and 0.1 mM EDTA. Other chemicals were reagent grade or better and were used without purification.

Antibiotic solutions were prepared from methanol stock solutions stored at −20 °C. Concentrations of stock solutions were determined from the absorbance at 320 nm with ϵ_{320} = 3600 M^{-1} cm^{-1} for TME (Arima et al., 1972) and ϵ_{320} = 3650 M^{-1} cm^{-1} for MTME (Barkley et al., 1986). An aliquot of the stock solution was placed in a vial, and the methanol was evaporated by a stream of N_2. Buffer was added to give the desired final concentration. The solution was equilibrated overnight at 4 °C to convert the methyl ether to the carbinolamine. DNA adducts were prepared by adding calf thymus DNA solution (2.5×10^{-3} M nucleotide) to give P/D = 100. The reaction was equilibrated for 2 or more days at 4 °C and then overnight at room temperature prior to measurement.

Absorbance and Fluorescence Measurements. Samples were placed in 1-cm stoppered cells and were thermostated by a circulating water bath. Absorbance was measured in a Cary 118 spectrophotometer. Fluorescence was measured in a SLM 8000 spectrofluorometer equipped with single excitation and emission monochromators and interfaced to an Apple II+ microcomputer. Magic-angle polarizers were set to 55° on the excitation side and 0° on the emission side, which minimizes the Woods anomaly of the emission grating. Fluorescence data were acquired in the ratio mode, and background fluorescence from a solvent blank was subtracted. Emission spectra were corrected for wavelength-dependent instrument response by using correction factors determined with a standard lamp from Optronics. The absorbance of solutions was <0.1 at the long-wavelength maximum. Photobleaching of antibiotics bonded to DNA was noted after lengthy exposure to the excitation beam in the SLM fluorometer. Photolysis was avoided by setting the excitation slits at 1-nm bandpass for fluorescence measurements on DNA adducts.

Quantum Yields. Fluorescence quantum yields were determined relative to quinine sulfate at a 337-nm excitation wavelength. A fresh solution of quinine bisulfate (Eastman Kodak) was prepared by dissolving a few crystals in 1 N H_2SO_4 (double distilled, GFS Chemicals) and adjusting the absorbance to <0.07 at 350 nm. A quantum yield of 0.546 at 25 °C with a temperature dependence of −0.25%/°C was used for quinine sulfate (Melhuish, 1961). Errors in quantum yields were about 10%. The temperature dependence of the quantum yield ϕ was fit to an Arrhenius equation (Kirby & Steiner, 1970).

$$\phi^{-1} - 1 = \sum_i (A_i/k_r) \exp(-E_i/RT) \qquad (1)$$

where A_i and E_i are the frequency factors and activation energies for nonradiative decay processes, R is the gas constant, and T is the absolute temperature. Equation 1 assumes that the radiative rate k_r is independent of temperature.

Titrations. pH titrations were done at 25 °C by adding small aliquots of concentrated H_3PO_4 or NaOH to solutions prepared in 0.01 M phosphate buffer, 0.1 M NaCl, and 0.1 mM EDTA. Titrations were monitored by absorbance and fluorescence. The absorbance of antibiotic solutions was measured at 284 nm. DNA absorbance was measured at 260 nm on 30- to 100-fold dilutions of DNA-adduct solutions. Hyperchromicity at 260 nm was calculated from $[A(\text{pH}) - A(\text{pH } 7.5)]/A(\text{pH } 7.5)$. The fluorescence intensity of antibiotic solutions was measured at a 337-nm excitation wavelength (4-nm bandpass) and a 410-nm emission wavelength (4-nm bandpass). The absorbance of the tomaymycin solution at pH 11 was <0.1 at 315 nm. Fluorescence intensity of 3- to 10-fold dilutions of DNA-adduct solutions was measured at 313-, 337-, and 350-nm excitation wavelengths and a 410-nm emission wavelength (8-nm bandpass).

Solute Quenching. The fluorescence intensity was monitored as a function of quencher concentration at 25 °C. Small aliquots of the following stock solutions were added: 1 M acrylamide (ultrapure, Schwarz/Mann Biotech) in buffer containing NaCl at the indicated concentration; 1 M NaI; 0.1 M $NaNO_3$; 1 M CsCl (optical grade, Kawecki Berylco Industries); 0.1 M $AgNO_3$ (99.9%+); 0.1 M $EuCl_3$ (99.99%, Aldrich); or 0.1 M $TbCl_3$ (99.99%, Aldrich). All experiments except the ones with lanthanides were performed at constant ionic strength. The intensities were measured at a 337-nm excitation wavelength and a 410-nm emission wavelength for three 10-s intervals, and the values were averaged. Quenching data were fit to the modified form of the Stern–Volmer equation

$$F_0/F = (1 + K_{SV}[Q])e^{V[Q]} \qquad (2)$$

where F_0 and F are the fluorescence intensities in the absence and presence of quencher Q, K_{SV} is the Stern–Volmer constant, and V is a static quenching constant (Eftink & Ghiron, 1981). Quenching parameters were determined by least-squares analysis. Linear Stern–Volmer plots were fit assuming V = 0 in eq 2.

Molecular Modeling Calculations. The crystal structure of TME (Arora, 1981) without the 11-methoxy group was taken as the initial structure. Partial atomic changes were

determined from ab initio calculations using GAUSSIAN-80 UCSF (Singh & Kollman, 1984) as described previously (Cheatham et al., 1988). Two different forms of 11-demethoxy-TME were constructed: one with an intramolecular H-bond between HO8 and O7 and one with the 8-hydroxyl rotated to a perpendicular position. Both forms were minimized with the program AMBER 3.0 (Singh et al., 1986) with all-atom force-field parameters (Weiner et al., 1984) and a distance-dependent dielectric constant. Parameters for the additional atom types present in tomaymycin were taken from the crystal structure (bond lengths, bond angles, and torsional angles). Structures were refined until the rms gradient was <0.1 kcal/mol Å. The two minimized structures had equal enthalpies of +21.0 kcal/mol. The structure of 8-*O*-methyltomaymycin was obtained by replacing the 8-phenolic proton of the second 11-demethoxy-TME structure with a methyl group. Partial atomic charges on the 8-methoxyl group and the C8 carbon were estimated from charges on the 7-methoxyl group and the requirement that the molecule be uncharged. Minimization of this structure gave an enthalpy of +26.0 kcal/mol. Minimized structures of the tomaymycin species were docked at GUA3 on the 6-mer duplex d-$(ATGCAT)_2$ with the aid of the interactive graphics program MIDAS (Ferrin et al., 1988a,b). The structures of the resulting adducts were minimized by using AMBER 3.0 and parameters therein for the nucleotides. They were then subjected to two consecutive 10-ps runs of molecular dynamics during which the DNA was held stationary and the drug was allowed to move (belly dynamics) as the temperature was raised from 10 to 300 K. The step length was 0.001 ps, the nonbonded cutoff was 10 Å, and the nonbonded pair list was updated every 20 steps. The boundary condition of constant temperature was imposed for equilibration. Structures obtained from the dynamics were refined further with molecular mechanics, with a distance-dependent dielectric constant and a nonbonded cutoff of 99 Å (to include all atoms) and with an update of the nonbonded pair list every 20 cycles. Periodic boundary conditions were not used. It was necessary to hold the DNA stationary during the dynamics because the $d(ATGCAT)_2$ frays at the ends and does not reform the terminal Watson–Crick base pairs on subsequent molecular mechanics refinement. For each adduct, a helix generated from Arnott's B-DNA geometry (Arnott et al., 1976) was also minimized (no drug present). The helix distortion enthalpy was determined by subtracting the enthalpy of the helix alone from the enthalpy of the helix in the adduct. The drug distortion enthalpy was determined by subtracting the enthalpy of the separately minimized drug from the enthalpy of the drug in the adduct.

For calculations with counterions and solvent, sodium ions were placed on the phosphate bisector 3.0 Å from the phosphorus atom (Seibel et al., 1985). A sphere of radius 1.65 Å was used for the sodium ions, and the distance between these ions and any atoms in the adducts was limited to 2.0 Å. While there is no room for water molecules between sodium and phosphate ions, this arrangement allows solvation of both ions on their perimeters. The resulting complex was solvated in a box of TIP3P water (Jorgensen et al., 1983) to a minimum solvent shell thickness of 4 Å, and any water was discarded if its oxygen was <2.0 Å or hydrogen was <1.0 Å from a solute atom. These conditions gave solvent boxes of (31.4–33.1) × (30.8–32.3) × (27.0–28.3) Å containing 675–740 water molecules depending on the adduct. Complete solvation of the DNA minor groove required molecular dynamics, which was done by allowing the water to move for two consecutive 10-ps periods while holding the DNA constant. Solvated structures obtained from the dynamics were then refined by molecular mechanics with all atoms free to move until the rms gradient was <0.2 kcal/mol Å. A uniform dielectric constant of 1.0 was used. Other parameters were the same as given above.

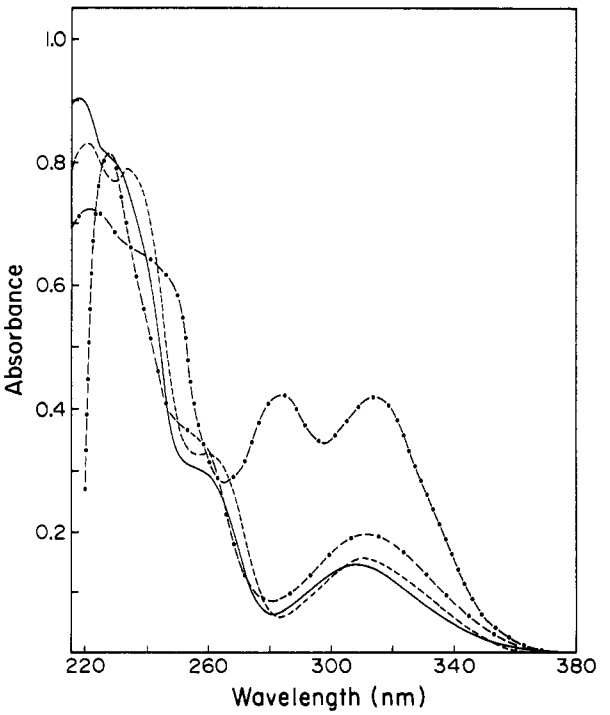

FIGURE 3: Absorption spectra of tomaymycin and 8-*O*-methyltomaymycin. Shown are tomaymycin at (—) pH 5 and (-·-) pH 11; 8-*O*-methyltomaymycin at (---) pH 5 and (-··-) pH 11. Conditions: 4.3×10^{-5} M antibiotic, 0.01 M phosphate buffer, 0.1 M NaCl, and 0.1 mM EDTA, 25 °C.

The computational protocol of holding the DNA coordinates constant during molecular dynamics simulations may limit the reliability of the net binding enthalpies in Table V. However, this limitation is at least partly overcome by the subsequent molecular mechanics refinement. Although variations in net binding enthalpies at other simulation times were not investigated, no significant differences in visual representations of the conformations were seen after 10 and 20 ps of dynamics. It seems unlikely that allowing DNA movement during the dynamics would produce significant changes in the solvation of the drug, which involves only the exposed O5, O7, O8, and HO8 atoms. Subtle changes in the solvation of the DNA are more likely.

RESULTS

Absorbance. The absorption spectra of tomaymycin at pH 5 and 11 are shown in Figure 3. The spectrum at pH 5 has a peak at 218 nm with shoulders at about 230 and 260 nm and a broad peak at 309 nm. The large extinction coefficients at the maxima, $\epsilon_{218} = 2.1 \times 10^4$ M^{-1} cm^{-1} and $\epsilon_{309} = 3.4 \times 10^3$ M^{-1} cm^{-1} (Barkley et al., 1986), indicate $\pi \rightarrow \pi^*$ transitions. The spectrum of the carbinolamine formed by hydrolysis of TME in aqueous solution is similar in appearance to the spectrum of TME in methanol (Arima et al., 1972). The peaks are shifted 6–10 nm to the blue, the shoulders are less pronounced, and the absorbance is decreased somewhat in the carbinolamine compared to the 11-methyl ether. At alkaline pH the shape of the spectrum changed markedly, and the extinction coefficient at the long-wavelength maxima increased almost 3-fold. The spectrum at pH 11 has a peak at 220 nm, a broad shoulder at about 240 nm, and two peaks at

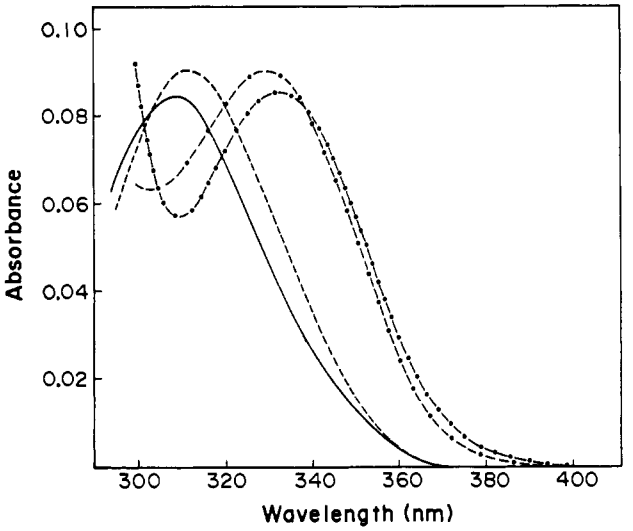

FIGURE 4: Absorption spectra of calf thymus DNA adducts. Shown are (—) tomaymycin and (-·-) the tomaymycin–DNA adduct, P/D = 100; (---) 8-*O*-methyltomaymycin and (—·—) the 8-*O*-methyltomaymycin–DNA adduct, P/D = 100. Conditions: 2.5×10^{-5} M antibiotic, 2.5×10^{-3} M nucleotide, 0.01 M cacodylate buffer, pH 6.4, 0.1 M NaCl, and 0.1 mM EDTA, 25 °C.

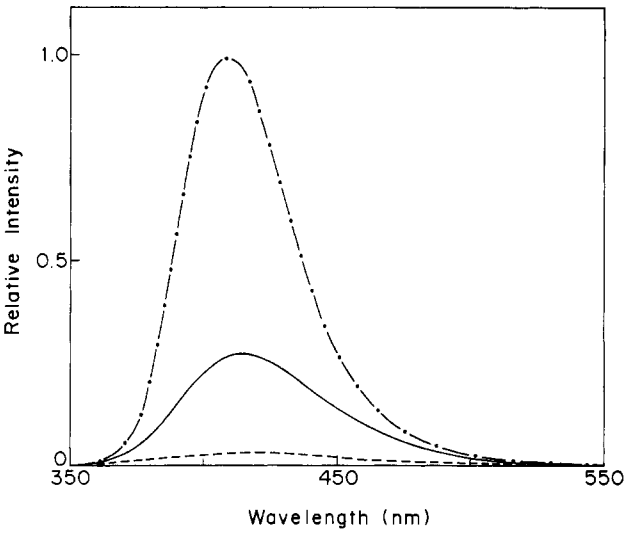

FIGURE 5: Emission spectra (8-nm bandpass) of tomaymycin and the tomaymycin–DNA adduct. Shown are (—) tomaymycin at λ_{ex} = 309 nm and (-·-) the tomaymycin–DNA adduct, P/D = 100, at λ_{ex} = 330 nm, 2.5×10^{-5} M tomaymycin, 2.5×10^{-3} M nucleotide, 0.01 M cacodylate buffer, pH 6.4, 0.1 M NaCl, and 0.1 mM EDTA, 25 °C, (---) tomaymycin at λ_{ex} = 309 nm, 2.5×10^{-5} M tomaymycin, 0.01 M phosphate buffer, pH 11, 0.1 M NaCl, and 0.1 mM EDTA, 25 °C.

284 and 315 nm. These spectral changes are due to the 8-hydroxyl on the aromatic ring of tomaymycin. The absorption spectrum of 8-*O*-methyltomaymycin, which lacks the phenolic proton, is similar to the spectrum of tomaymycin at pH 5 but does not undergo analogous changes at higher pH (Figure 3). The absorption spectral changes of tomaymycin were reversible over the range of pH 4.4–11.4 with isosbestic points at about 240 and 262 nm. This indicates predominantly two ground-state species in aqueous solution: the phenol and phenolate anion. Previously we showed that tomaymycin is an equilibrium mixture of 11S,11aS and 11R,11aS diastereomers in protic solvents (Barkley et al., 1986). The two diastereomers have slightly different absorption and emission spectra. In aqueous solution at pH 5 the carbinolamine is mostly the 11S,11aS diastereomer with perhaps a trace of the 11R,11aS diastereomer.

When tomaymycin is bonded to DNA, the long-wavelength absorption band is red-shifted to 331 nm (Nishioka et al., 1972). Figure 4 shows the absorption spectra of tomaymycin and the calf thymus DNA adduct at pH 6.4 and P/D = 100. All of the drug was reacted with DNA, as judged by solvent extraction and fluorescence lifetime measurements (Barkley et al., 1991). At this pH tomaymycin is 97% in the phenol form (see below). There was no change in the extinction coefficient at the long-wavelength maximum upon bonding to DNA, which implies that the bound drug has a protonated 8-hydroxyl. The absorption spectrum of 8-*O*-methyltomaymycin also showed about a 20-nm red shift after reaction with DNA (Figure 4). However, about 20% of the 8-*O*-methyltomaymycin was unbound under the same experimental conditions (Barkley et al., 1991). This suggests that the bulky methanol group at the 8-position of the aromatic ring partially interferes with DNA bonding.

Fluorescence Emission. The emission spectra of tomaymycin and the calf thymus DNA adduct excited at the long-wavelength absorption maxima are depicted in Figure 5. The spectra of tomaymycin and 8-*O*-methyltomaymycin (not shown) at pH 6.4 are almost identical, with broad peaks at 411 and 413 nm, respectively, but the fluorescence quantum yield of 8-*O*-methyltomaymycin is slightly higher (Barkley et al., 1986). At pH 11 the fluorescence of tomaymycin was almost completely quenched with no shift in the emission band. The fluorescence intensity changes of tomaymycin were reversible over the range of pH 4.4–11.4. This contrasts with 8-*O*-methyltomaymycin which undergoes a large irreversible increase in fluorescence intensity accompanied by a small blue shift in the emission band above pH 8. Anthramycin is also unstable in basic solution at room temperature (Kohn & Spears, 1970).

The fluorescence of tomaymycin is enhanced upon bonding to DNA (Maruyama et al., 1979). The peak intensity increases almost 4-fold and the emission band shifts about 4 nm to the blue in the calf thymus DNA adduct (Figure 5). 8-*O*-Methyltomaymycin fluorescence showed similar changes with somewhat greater enhancement when bonded to DNA (Barkley et al., 1986). The emission intensity of the DNA adducts decreased with increasing temperature in a range well below the DNA melting transition. The T_m for the tomaymycin–DNA adduct at P/D = 100 was 82 °C. The absorption spectrum of bound tomaymycin did not change until about 50 °C. No shifting or broadening of the emission spectra of the adducts occurred from 5 to 40 °C, suggesting that higher temperature mostly affects the rates of deactivation but not the electronic properties of the excited state. The quantum yields of the tomaymycin– and 8-*O*-methyltomaymycin–DNA adducts were measured from 5–40 °C, and the temperature dependence was analyzed according to eq 1. In both cases the plots of ln $(\phi^{-1} - 1)$ vs $1/T$ were linear (not shown), indicating that a single Arrhenius term is sufficient to fit the data. This implies that the excited state is deactivated by two pathways: a temperature-independent radiative decay and a temperature-dependent nonradiative process. However, because of the narrow temperature range and scatter in the data, we cannot exclude additional temperature-independent and temperature-dependent decay routes. The activation energy E of the temperature-dependent process was 4.3 kcal/mol for the tomaymycin adduct and 3.4 kcal/mol for the 8-*O*-methyltomaymycin adduct. These values are small compared to the 7.1 kcal/mol activation energy of tyrosine (Gally & Edelman, 1962).

pH Titrations. The absorbance and fluorescence intensity changes of tomaymycin are plotted as a function of pH in

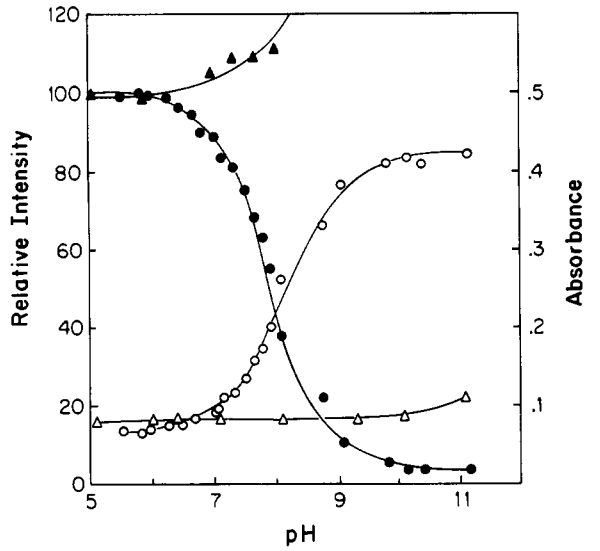

FIGURE 6: pH titration of (●, ○) tomaymycin and (▲, △) 8-*O*-methyltomaymycin. Shown are the emission intensity (filled symbols) at λ_{ex} = 313 nm, λ_{em} = 410 nm, and the absorbance (open symbols) at 284 nm, 0.10 M phosphate buffer, 0.1 M NaCl, and 0.1 mM EDTA, 25 °C.

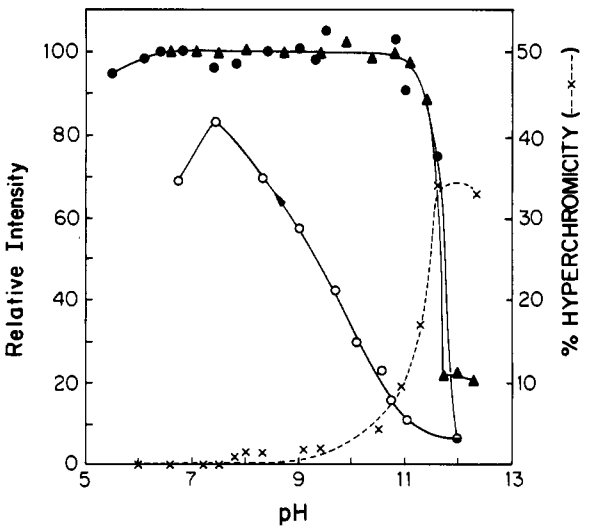

FIGURE 7: pH titration of calf thymus DNA adducts. Shown are the emission intensity of (●, ○) the tomaymycin–DNA adduct and (▲) the 8-*O*-methyltomaymycin–DNA adduct at λ_{ex} = 337 nm, λ_{em} = 410 nm, and (×) the absorbance of the tomaymycin–DNA adduct at 260 nm, 0.01 M phosphate buffer, 0.1 M NaCl, and 0.1 mM EDTA, 25 °C.

Figure 6. The ground-state pK determined from the absorbance change at 284 nm was 8.0, which is consistent with titration of the 8-phenolic proton. The pK of the 9-phenolic proton in anthramycin is about 8.7 (Kohn et al., 1974). In tomaymycin the 8-hydroxy is para to the electron-withdrawing 5-carbonyl, which stabilizes the phenolate anion by delocalization of the π orbitals and lowers the pK. The inflection point of the fluorescence intensity change was at pH 8.0 and was independent of buffer concentration, suggesting that the excited-state pK^* is likewise about 8.0. The excited-state pK^* of tomaymycin was estimated from the Förster cycle

$$pK - pK^* = Nhc(\bar{\nu}_{OH} - \bar{\nu}_{O^-})/2.303RT \quad (3)$$

where N is Avogadro's number, h is Planck's constant, c is the speed of light in the solution, and $\bar{\nu}_{OH}$ and $\bar{\nu}_{O^-}$ are the wave numbers of the transitions of the phenol and phenolate anion, respectively. The calculated value of pK^* is less than one pH unit below pK, whether $\bar{\nu}_{OH}$ and $\bar{\nu}_{O^-}$ are absorption maxima, the average of absorption and emission maxima, or emission maxima.

The fluorescence intensities of tomaymycin– and 8-*O*-methyltomaymycin–DNA were monitored as a function of pH (Figure 7). The emission of both DNA adducts remained almost constant until about pH 10.5. This suggests that the 8-phenolic proton is no longer titratable when tomaymycin is bonded to double-stranded DNA. The 9-phenolic proton of anthramycin is also stabilized in the DNA adduct (Kohn et al., 1974). Above pH 11 the emission intensity dropped abruptly. The fluorescence quenching was accompanied by an increase in DNA hyperchromicity due to alkaline denaturation of the double helix. The 5- to 10-fold decrease in fluorescence of the DNA adducts at high pH is not caused by release of drug from denatured DNA. First, the aminal linkage has considerable stability under alkaline conditions (Hurley et al., 1977). At pH 7.2–12, radiolabeled tomaymycin is not released from the calf thymus DNA adduct in 60 min at 23 °C, though 25% of the bound drug can be removed by dialysis at pH 11.0 for 48 h. In contrast, the fluorescence intensity drops occurred immediately in both the adducts. Second, the fluorescence titration curves of 8-*O*-methyltomaymycin–DNA adduct measured at 313-, 337-, and 350-nm excitation wavelength were similar. If 8-*O*-methyltomaymycin were released from DNA at alkaline pH, the fluorescence intensity at 313 nm should have increased about 3-fold due to decomposition of the unbound drug. Finally, the fluorescence titrations of the DNA adducts were partially reversible (Figure 7). Back titration immediately restored about 80% of the original emission intensity at pH 7.5. The DNA was not fully renatured as apparent from the hyperchromicity. The fluorescence intensity increases during back titration cannot be due to bonding of free antibiotic at renatured regions on DNA because the reaction kinetics are too slow (Barkley et al., 1991).

Solute Quenching. The accessibility of a chromophore to small solute molecules may be determined from fluorescence-quenching studies. The Stern–Volmer constant for collisional quenching K_{SV} is related to the bimolecular quenching rate constant k_q through

$$K_{SV} = k_q\tau_0 \quad (4)$$

where τ_0 is the fluorescence lifetime in the absence of the quencher. In cases where the efficiency of the quenching reaction is unity, the quenching rate is diffusion controlled and the interpretation of quenching data is straightforward (Eftink & Ghiron, 1981). The quenching efficiency γ is defined as a proportionality factor

$$k_q = \gamma k_d \quad (5)$$

where k_d is the diffusion-controlled rate constant. Values of k_d may be estimated from the steady-state term in the Smoluchowski equation

$$k_d = 4\pi NrD/1000 \quad (6)$$

where r is the collision radius and D is the sum of the diffusion coefficients of the fluorophore and quencher.

Several common fluorescence quenchers were tested for their ability to quench tomaymycin fluorescence. Figure 8 shows a Stern–Volmer plot of acrylamide quenching data. The upward curvature at higher acrylamide concentrations indicates static quenching. The quenching data in the linear region below 0.2 M acrylamide were fit to the Stern–Volmer equation (eq 2 with V = 0). A bimolecular quenching rate constant k_q of about 8×10^9 M^{-1} s^{-1} at 25 °C was obtained, which is close to the diffusion-controlled rate. Nonlinear fits of

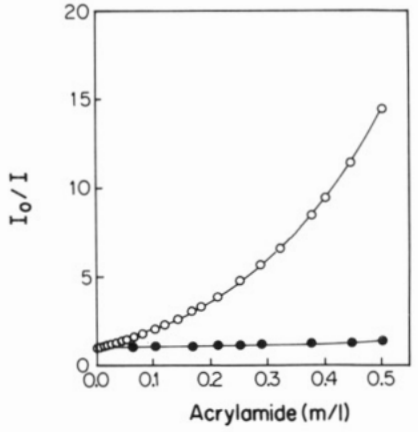

FIGURE 8: Stern–Volmer plots of fluorescence of tomaymycin and the tomaymycin–DNA adduct quenched by acrylamide. Shown are (○) tomaymycin, 0.01 M cacodylate buffer, pH 5.9, 0.1 M NaCl, and 0.1 mM EDTA, and (●) the tomaymycin–DNA adduct, P/D = 100, 0.01 M cacodylate buffer, pH 6.4, 0.1 M NaCl, and 0.1 mM EDTA. Conditions: λ_{ex} = 337 nm, 25 °C.

Table I: Quenchers of Tomaymycin Fluorescence[a]

quencher	$k_q \times 10^{-9}$ (M^{-1} s^{-1})	V (M^{-1})	γ[b]	conditions[c]
neutral acrylamide				
	7.9		1.0	pH 5.9, 0.1 M NaCl
	5.4	2.6	0.7	
	7.8		1.0	pH 5.9, 1.0 M NaCl
	6.7	0.6	0.9	
	8.6		1.1	pH 5.9, 5.0 M NaCl
	6.9	0.8	0.9	
	7.9		1.0	pH 7.5, 0.1 M NaCl
	5.8	1.1	0.8	
	8.2		1.1	pH 7.5, 5.0 M NaCl
	6.2	1.1	0.8	
anions				
I^-	1.1		0.1	pH 5.9, 1.0 M NaCl
NO_3^-	3.5		0.5	pH 5.9, 0.1 M $NaClO_4$
cations				
Cs^+	0.08		0.01	pH 5.9, 1.0 M NaCl
Ag^+	15.5		2.1	pH 5.9, 0.1 M $NaClO_4$
	7.8	5.4	1.0	
Eu^{3+}	11.2		1.5	pH 5.1, 0.1 M NaCl
Tb^{3+}	10.3		1.4	pH 5.1, 0.1 M NaCl

[a] Conditions: λ_{ex} = 337 nm; λ_{em} = 414 nm; 25 °C. The k_q values were calculated with τ_0 = 1.1 ns (Barkley et al., 1986). [b] Estimated from eqs 6 and 7. Ionic radii were calculated by assuming one hydration shell. Diffusion coefficients were calculated from the Stokes–Einstein equation. [c] pH 5.1 and pH 5.9 buffers are 0.01 M cacodylate; pH 7.5 buffer is 0.01 M phosphate.

quenching data up to 0.5 M acrylamide gave slightly lower k_q values with static quenching constants V of 1–3 M^{-1}. Such values of the static quenching constant are typical of transient effects occurring within about a 10-Å radius of the fluorophore (Eftink & Ghiron, 1976; Andre et al., 1978). Acrylamide appears to quench tomaymycin fluorescence with nearly unit efficiency under several solution conditions (Table I). In contrast, the two anionic quenchers tested: I^- and NO_3^- were relatively poor quenchers with efficiencies of 0.1 and 0.5, respectively. Tomaymycin fluorescence was not quenched by Cs^+, though it was quenched with high efficiency by other metal cations: Ag^+, Eu^{3+}, and Tb^{3+}. The quenching constants for $AgNO_3$ include contributions from both the Ag^+ and NO_3^- ions. The large value of the static quenching constant V suggests that Ag^+ binds to tomaymycin. The transition metal and lanthanide ions are not good choices for quenching experiments with DNA because they bind to the DNA bases causing aggregation at higher concentrations (Marzilli, 1976).

Table II: Acrylamide Quenching of Fluorescence of Tomaymycin–DNA Adducts[a]

adduct	[NaCl] (M)	K_{SV} (M^{-1})	$\langle\tau_0\rangle$ (ns)	$k_q \times 10^{-9}$ (M^{-1} s^{-1})
TOM	0.1	0.86	4.99	0.17
	5.0	0.87	4.99	0.17
MTOM	0.1	0.68	6.87	0.10
	5.0	0.76	6.87	0.11

[a] Conditions: λ_{ex} = 330 nm, λ_{em} = 420 nm, 25 °C. 0.01 M phosphate buffer, pH 7.5, 0.1 M NaCl or 5.0 M NaCl, 0.1 mM EDTA. $\langle\tau_0\rangle$ values are from Barkley et al. (1991).

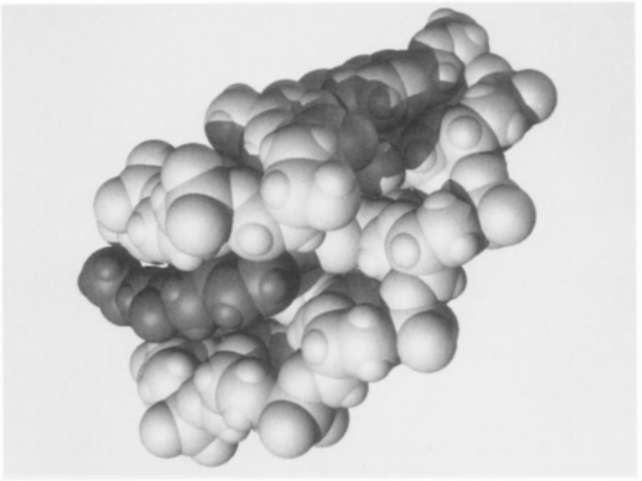

FIGURE 9: Space-filling model of the S5′ tomaymycin–d(ATGCAT)$_2$ adduct.

The accessibility of tomaymycin and 8-*O*-methyltomaymycin bonded to DNA was probed by acrylamide. The Stern–Volmer plots of the DNA adducts were linear (Figure 8). The quenching parameters are given in Table II. The values of about 0.1 × 10^9 M^{-1} s^{-1} for k_q are nearly 50-fold lower than the diffusion-controlled rate estimated for a sphere the size of tomaymycin immobilized on DNA. The small quenching rate constants indicate that the aromatic ring of the antibiotic is almost completely shielded from the solvent in the DNA adduct.

Molecular Modeling. The interaction of tomaymycin and 8-*O*-methyltomaymycin with DNA was modeled with the molecular mechanics program AMBER 3.0. Each antibiotic was attached by a covalent bond to the N2 of guanine in a B-form 6-mer duplex. The sequence d(ATGCAT)$_2$ was chosen because it mimics calf thymus DNA in forming both 11S and 11R diastereomeric adducts with tomaymycin (Barkley et al., 1986; Cheatham et al., 1988). Calculations were performed for the four possible binding modes: S or R configuration at the drug covalent-linkage site with 3′ or 5′ orientation of the aromatic ring along the DNA strand. The models are identified by configuration and direction. For example, S3′ refers to the model with S configuration at the drug C11 and the aromatic ring pointing toward the 3′ end of the covalently bonded DNA strand. Relative binding enthalpies for the four different models of the tomayamycin– and 8-*O*-methyltomaymycin–d(ATGCAT)$_2$ adducts were first determined by energy minimization in a vacuum with a distance-dependent dielectric constant. Tomaymycin species with and without an intramolecular H-bond between HO8 and O7 were used in the calculations. The species with the intramolecular H-bond always gave a lower enthalpy adduct. Only those tomaymycin adducts with the HO8–O7 H-bond are listed in Table III and discussed below. In all models of the adducts, the aromatic ring was highly shielded above and below by base and sugar

Table III: Binding Enthalpies (kcal/mol) for Tomaymycin- and 8-*O*-Methyltomaymycin–d(ATGCAT)$_2$ Adducts in a Vacuum

adduct	config and direction	total	helix in adduct	helix distort.[a]	drug in adduct	drug distort.[b]	total intermol[c]	net binding[d]
TOM	S3′	−403.0	−389.7	12.5	21.2	0.2	−34.3	−21.6
	S5′	−408.7	−394.2	8.0	21.5	0.5	−37.4	−28.9
	R3′	−388.4	−386.4	15.8	29.5	8.5	−31.5	−7.2
	R5′	−403.9	−395.5	6.7	26.9	5.9	−36.6	−24.0
MTOM	S3′	−391.6	−383.3	18.9	29.0	3.0	−37.3	−15.4
	S5′	−389.2	−389.3	12.9	27.7	1.7	−36.6	−22.0
	R3′	−384.7	−386.2	16.0	35.1	9.1	−33.6	−8.5
	R5′	−393.4	−390.2	12.0	35.1	9.1	−38.3	−17.2

[a] The helix distortion enthalpy is the enthalpy of the helix in the adduct minus the enthalpy of the helix minimized alone. The lowest value from all of the separate minimizations was used (−402.2 kcal/mol). [b] The drug distortion enthalpy is the enthalpy of the drug in the adduct minus the enthalpy of the drug minimized alone (21.0 kcal/mol for tomaymycin and 26.0 kcal/mol for 8-*O*-methyltomaymycin). [c] The total intermolecular binding enthalpy is the sum of the electrostatic and van der Waals interactions. [d] The net binding enthalpy is the total intermolecular binding enthalpy plus the helix and drug distortion enthalpies.

Table IV: Interaction Enthalpies (kcal/mol) for Tomaymycin with Individual Residues of d(ATGCAT)$_2$[a]

config and direction	GUA3	P3,4	CYT4	P4,5	CYT10	SUGAR11	ADE11	SUGAR12
S3′		−3.1	−2.8	−6.1	−2.5	−2.7	−2.8	
		(−3.4)	(−0.5)	(−3.9)	(−1.1)	(−0.5)	(−0.9)	
S5′		−3.6	−2.5		−2.8		−6.6	−3.3
		(−2.2)	(−1.3)		(−1.5)		(−3.9)	(−0.2)
R5′	−3.0		−2.8		−2.5	−2.5	−7.3	
	(−2.6)		(−1.2)		(−1.4)	(−0.5)	(−4.4)	

[a] Only interactions stronger than −2.5 kcal/mol are included. The component of enthalpy attributed to electrostatics is given in parenthesis below the total interaction enthalpy. The remainder of the enthalpy is attributed to van der Waals forces. Most of the enthalpy of hydrogen bonds is in the electrostatic term.

Table V: Binding Enthalpies (kcal/mol) for Tomaymycin- and 8-*O*-Methyltomaymycin–d(ATGCAT)$_2$ Adducts in the Presence of Water and Counterions[a]

adduct	config and direction	helix distort.[b]	drug distort.[c]	total intermol[d]	net binding[e]	drug-water (in adduct)
TOM	S3′	19.8	2.4	−31.0	−8.8	−21.8
	S5′	1.3	1.2	−32.9	−30.4	−25.6
	R3′	18.0	11.4	−28.3	+1.1	−14.3
	R5′	14.7	6.4	−34.4	−13.3	−22.8
MTOM	S3′	18.0	4.4	−28.3	−5.9	−14.3
	S5′	2.0	6.5	−33.8	−25.3	−22.7
	R3′	12.5	9.8	−28.8	−6.5	−17.4
	R5′	6.3	6.9	−37.0	−23.8	−21.2

[a] A solvated counterion with a 6-Å radius was placed at the bisector of each phosphate ion. Solvent was generated from 27 216 water cubes with a 4.0-Å cutoff criterion for discarding water. [b] The helix distortion enthalpy is the enthalpy of the helix in the adduct minus the enthalpy of the helix minimized in the same solvent system (−358.7 kcal/mol). [c] The drug distortion enthalpy is the enthalpy of the drug in the adduct minus the enthalpy of the drug minimized alone (21.0 kcal/mol for tomaymycin and 26.0 kcal/mol for 8-*O*-methyltomaymycin). [d] The total intermolecular binding enthalpy is the sum of electrostatic and van der Waal interactions. [e] The net binding enthalpy is the total intermolecular binding enthalpy plus helix and drug distortion enthalpies.

residues about the DNA minor groove. Figure 9 illustrates the shielding for the S5′ adduct of tomaymycin. Presumably this accounts for the low acrylamide quenching rate constants of the DNA adducts.

Table III gives the enthalpies obtained from the minimization in a vacuum. Net binding enthalpies were calculated by adding the helix and drug distortion enthalpies to the total intermolecular binding enthalpy. These distortion enthalpies arise from the induced fit between the drug and the DNA that occurs in order to optimize intermolecular interactions. The enthalpy of the aminal linkage was assumed to be constant and was neglected. In all cases the length of this C–N bond was 1.47 Å. The relative net binding enthalpies for the four models of the tomaymycin adduct parallel those for the corresponding models of the 8-*O*-methyltomaymycin adduct. It is clear that the S5′ geometry is preferred by both antibiotics. There is little structural difference between adducts of the two drugs having the same configuration and minor-groove orientation. For example, least-squares fitting of the models of the tomaymycin and 8-*O*-methyltomaymycin adducts with S5′ geometry gave an rms deviation of only 0.03 Å for all atoms except the O8 substituent of the drug. The net binding enthalpies in Table III favor tomaymycin over 8-*O*-methyltomaymycin

Table IV lists the enthalpies for the most important interactions of tomaymycin with individual residues of d-(ATGCAT)$_2$. The R3′ model was not examined. The other binding modes showed strong interactions with bases in a three base pair sequence: CYT4 on the covalently modified strand and CYT10 and ADE11 on the opposite strand. However, the pattern of interactions is unique for each geometry. Electrostatic interactions <−2.5 kcal/mol with phosphates occurred only in the S3′ adduct. The van der Waals interactions <−2.5 kcal/mol occurred with ADE11 and deoxyribose of THY12 in the S5′ adduct and with ADE11 in the R5′ adduct. These include interactions between the C2 proton of ADE11 and the C9 and N10 protons of tomaymycin plus interactions with N3 and C2 of ADE11. The sugar interactions involve H1′ and O1′ of deoxyribose and C9a and C11 of tomaymycin.

The tomaymycin and 8-*O*-methyltomaymycin adducts were further studied by including solvation water and counterions for the DNA phosphate anions in the models. This was done by immersing the adducts previously minimized in a vacuum

Table VI: Hydrogen-Bond Parameters of Solvated Tomaymycin- and 8-*O*-Methyltomaymycin–d(ATGCAT)$_2$ Adducts[a]

adduct	config and direction	hydrogen donor (X–H)	acceptor atom (Z)	length (Å)	angle (deg)
TOM	S3′	N10–HN10 (TOM)	O2 (CYT10)	2.30	147.8
		O8–HO8 (TOM)	O (WAT)[b]	2.08	137.3
		O–H (WAT)	O7 (TOM)	2.39	128.1
		O–H (WAT)	O5 (TOM)	1.88	149.5
	S5′	N10–HN10 (TOM)	N3 (ADE11)	1.97	155.6
		O8–HO8 (TOM)	O7 (TOM)	2.24	114.3
		O–H (WAT)	O8 (TOM)	2.36	129.4
		O–H (WAT)	O7 (TOM)	1.95	165.9
		O–H (WAT)	O5 (TOM)	1.90	167.8
		O–H (WAT)	O5 (TOM)	1.91	164.7
	R3′	N10–HN10 (TOM)	O2 (CYT4)	1.97	165.9
		O8–HO8 (TOM)	O7 (TOM)	2.26	113.2
		O–H (WAT)	O5 (TOM)	1.87	171.1
	R5′	N10–HN10 (TOM)	N3 (ADE11)	1.93	174.5
		O8–HO8 (TOM)	O7 (TOM)	2.22	115.2
		O–H (WAT)	O5 (TOM)	1.91	169.5
		O–H (WAT)	O5 (TOM)	1.92	165.6
MTOM	S3′	N10–HN10 (MTO)	O2 (CYT10)	1.97	156.7
		O–H (WAT)	O7 (MTO)	1.95	152.9
		O–H (WAT)	O5 (MTO)	1.81	162.5
	S5′	N10–HN10 (MTO)	N3 (ADE11)	1.97	153.5
		O–H (WAT)	O7 (MTO)	1.94	166.2
		O–H (WAT)	O5 (MTO)	1.96	162.4
		O–H (WAT)	O5 (MTO)	2.32	116.0
	R3′	N10–HN10 (MTO)	O2 (CYT4)	1.98	171.0
		O–H (WAT)	O5 (MTO)	1.85	177.0
	R5′	N10–HN10 (MTO)	N3 (ADE11)	1.96	173.6
		O–H (WAT)	O7 (MTO)	1.98	166.6
		O–H (WAT)	O5 (MTO)	1.93	170.7
		O–H (WAT)	O5 (MTO)	1.96	174.6

[a] In a hydrogen bond X–H···Z, X and Z are the donor and acceptor atoms, respectively, the hydrogen-bond length corresponds to the distance between H and Z, and the angle is X–H···Z. [b] The water whose O is an acceptor for the H-bond from O8 of TOM acts as a donor to O3′of CYT10, thus forming a bridge between tomaymycin and DNA. The O–H···O3′ H-bond has a length of 2.05 Å and an angle of 168.5°.

into a box of TIP3P water and placing sodium ions on the bisector of each phosphate group in the DNA. The resulting structures were minimized with a uniform dielectric constant. The geometries changed only a little upon solvation. Table V gives values for the net binding enthalpy of the drug–duplex adducts, along with the total intermolecular binding enthalpy and the helix and drug distortion enthalpies. The total enthalpies of the system comprised of drug, duplex, counterions, and water molecules are not given in the table because they cannot be directly compared. The systems contain different numbers of water molecules, as a consequence of trimming the original box of water down to a size that can be calculated in a reasonable time and removing water molecules that would impinge upon the space occupied by the solute. The net binding enthalpies in Table V favor tomaymycin over 8-*O*-methyltomaymycin in the S adducts but not in the R adducts. The final column of Table V gives the intermolecular binding enthalpy between the bound drug and solvent molecules. These enthalpies may also influence the relative stabilities of the adducts. They favor the S5′ and R5′ adducts of tomaymycin over the corresponding adducts of 8-*O*-methyltomaymycin by small amounts. The S3′ adduct of tomaymycin is favored by 7.5 kcal/mol, possibly because of a unique water bridge to the DNA (Figure 10).

Specific hydrogen-bond formation is expected to be important in determining the stability and solvation of the tomaymycin- and 8-*O*-methyltomaymycin–d(ATGCAT)$_2$ adducts. In a vacuum the only H-bonds (other than Watson–Crick) in the adducts are the intramolecular HO8–O7 H-bond of tomaymycin and the intermolecular H-bonds between the N10 hydrogen and acceptor atoms on proximate bases: N3 of ADE11 for S5′ and R5′ adducts, O2 of CYT10 for S3′ adduct, and O2 of CYT4 for R3′ adduct. The addition of water molecules provides further opportunities for hydrogen

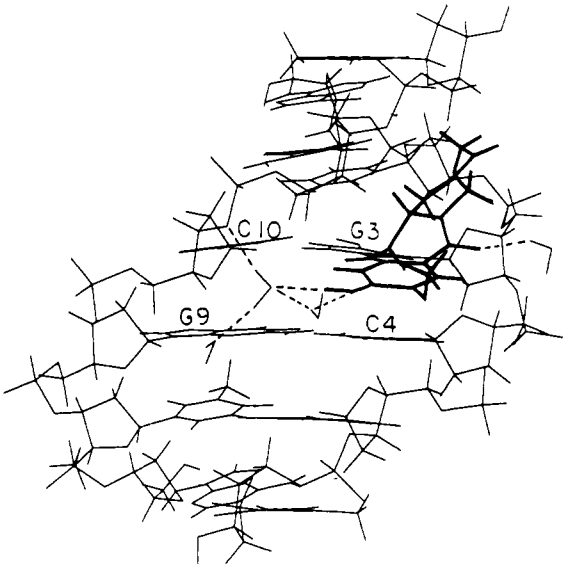

FIGURE 10: Diagram of the S3′ tomaymycin–d(ATGCAT)$_2$ adduct showing the water bridge between HO8 of tomaymycin and O3′ of CYT10. Dashed lines represent H-bonds.

bonding. Table VI lists the complete set of H-bonds for the solvated adducts. For the 8-*O*-methyltomaymycin adducts, water molecules bind to the drug O5 in all four binding modes with two H-bonds to O5 in the 5′ orientation and one in the 3′ orientation. A single H-bond is made to O7 in all but the R3′ adduct, which has none. Similar hydrogen-bonding patterns are found in the corresponding tomaymycin adducts along with others involving the 8-hydroxyl. A water molecule makes an H-bond with O8 in the S5′ adduct. The intramolecular H-bond between HO8 and O7 occurs in all but the S3′ adduct, which features instead a unique H-bond between HO8

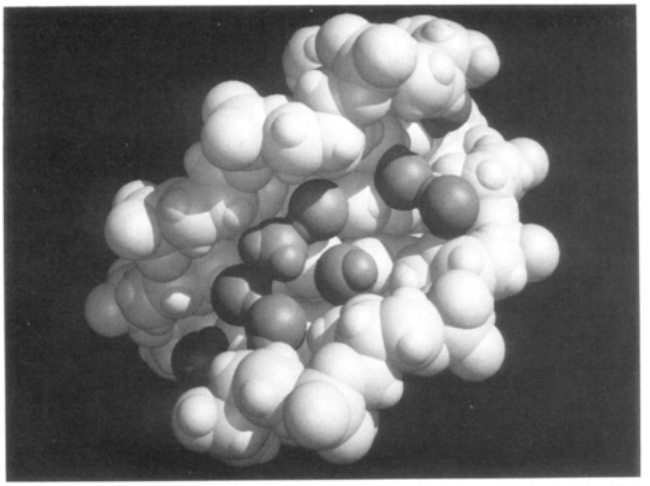

FIGURE 11: Space-filling model of the d(ATGCAT)$_2$ duplex showing first-shell waters in the minor groove. Waters are listed from the top and left to right in the following order: 426, 389, 356, 423, 394, 568, 691, 362, 645, and 668.

and oxygen of a water molecule. As seen in Figure 10, this water in turn forms an H-bond to O3′ of CYT10, thus completing a bridge between tomaymycin and the DNA backbone.

For comparison, the solvation of tomaymycin and d(ATGCAT)$_2$ was also modeled. Calculations were performed on the 11S,11aS diastereomer of the carbinolamine and on the duplex alone as described above. The free drug showed seven intermolecular H-bonds to water with HO8, HN10, and HO11 as donors and O5, O8 (two H-bonds), and O11 as acceptors, as well as the intramolecular H-bond between HO8 and O7. The 8-phenolic proton made a bifurcated H-bond. Figure 11 depicts the first-shell waters in the minor groove of d(ATGCAT)$_2$. There are ten water molecules in the first shell, which form a regular water structure reminiscent of the "strings" running down the two walls of the minor groove of CCAAGATTGG (Prive et al., 1987). The width of the minor groove, defined as the shortest P–P distance across the opening minus 5.8 Å for two phosphate group radii, is not constant in d(ATGCAT)$_2$: P4–5 to P11–12, 6.43 Å and P5–6 to P10–11, 5.98 Å; P3–4 to P11–12, 6.02 Å and P4–5 to P10–11, 6.26 Å. The irregularities appear to reflect DNA sequence effects on the hydration pattern, because the groove width is uniform in the vacuum model (P4–5 to P11–12 and P5–6 to P10–11, 5.31 Å; P3–4 to P11–12, 6.00 Å and P4–5 to P10–11, 6.08 Å). The distances are less than the 7.2-Å width in CCAAGATTGG but considerably larger than the 3.7-Å width in CGCGAATTCGCG (Prive et al., 1987). Table VII lists the H-bonds formed between first-shell waters and nucleosides in the minor groove. Two waters (426 and 568) span two bases in interstrand bridges, and two waters (362 and 394) make bifurcated H-bonds between base n and the O1′ of deoxyribose ($n + 1$). Tomaymycin forms a single intermolecular H-bond between HN10 and a base in the duplex (Table VI) at one of the hydration sites (Table VII). In the S3′ adduct this displaces a base–sugar water bridge (362) and a base–base interstrand water bridge (568). The drug also perturbs the P–P distances (values for the vacuum model are in parentheses): P4–5 to P11–12, 6.33 (6.12) Å and P5–6 to P10–11, 4.85 (4.97) Å; P3–4 to P11–12, 7.86 (6.97) Å and P4–5 to P10–11, 6.61 (6.26) Å.

Table VII: Hydrogen Bonds in First Hydration Shell in the Minor Groove of d(ATGCAT)$_2$

hydrogen donor (H–X)	acceptor atom	length (Å)	angle (deg)
H1 (WAT668)	N3 (ADE1)	2.10	136.8
H2 (WAT691)	N3 (GUA3)	2.27	152.0
H1 (WAT389)	N3 (GUA9)	1.97	156.7
H1 (WAT362)	N3 (ADE11)	1.85	170.0
H1 (WAT645)	O2 (THY2)	1.83	149.4
H2 (WAT356)	O2 (CYT4)	1.86	158.6
H2 (WAT426)	O2 (THY6)	1.82	163.1
H1 (WAT426)	O2 (THY8)	1.87	151.7
H2 (WAT568)	O2 (CYT10)	1.86	156.0
HN2A (GUA3)	O (WAT568)	2.44	106.9
HN2B (GUA3)	O (WAT394)	1.91	163.3
HN2B (GUA9)	O (WAT389)	2.07	133.8
H1 (WAT668)	O1′ (THY2)	2.45	131.8
H2 (WAT423)	O1′ (CYT10)	1.90	163.3
H1 (WAT362)	O1′ (THY12)	1.85	153.3

Discussion

We find that the absorption and fluorescence changes in tomaymycin on bonding to DNA are somewhat greater than originally reported (Nishioka et al., 1972; Maruyama et al., 1979). This is due to proximity of the pK to neutral pH and to very slow binding kinetics (Barkley et al., 1990). The large red shift in the long-wavelength absorption band is a hallmark of the interaction of intercalating and groove-binding dyes with DNA. Löber (1981) proposed that the red shift is essentially a solvation effect, the change in environment of a dye molecule going from hydrated state to bound state being similar to the transfer from water to an organic solvent. Tomaymycin differs from reversibly binding dyes in two respects: (1) the chemical reactivity in protic solvents and DNA adducts and (2) the presence of two diastereomers with slightly different absorption and emission spectra. Nevertheless, the absorption and emission spectral shifts of tomaymycin in water, organic solvent (Barkley et al., 1986), and DNA adducts show the same trends as proflavine and support Löber's interpretation.

Judging from the strength of the long-wavelength absorption band, the radiative rate k_r of tomaymycin is about the same in the free and bound drug. Estimates of k_r from quantum yield and mean lifetime data, $k_r = \phi/\langle\tau\rangle$, give 6×10^7 s^{-1} for tomaymycin and (5–7) $\times 10^7$ s^{-1} for the calf thymus DNA adduct (Barkley et al., 1986). The fluorescence quantum yield $\phi = k_r/k$ is the ratio of the radiative rate to the total decay rate k, where $k = k_r + k_{nr}$. If k_r does not change, then the nonradiative rate k_{nr} must account for the 4-fold difference in the quantum yield of free and bound tomaymycin. In the case of ethidium, the large fluorescence enhancement upon intercalation into DNA was attributed to inhibition of an excited-state proton transfer to solvent (Olmsted & Kearns, 1977). Four nonradiative processes have been invoked to explain the photophysics of phenol and its derivatives: internal conversion, intersystem crossing, excited-state proton transfer, and photoionization (Creed, 1984). The dominant decay channel of gas-phase phenol is internal conversion (Sur & Johnson, 1986). However, introduction of a single H-bond in phenol–water and phenol dimer complexes renders internal conversion noncompetitive in deactivating the excited singlet state. Intersystem crossing is an efficient nonradiative decay channel of phenols in both gas and condensed phases (Sur & Johnson, 1986; Bishai et al., 1967). Although aromatic hydroxyl groups are often stronger acids in the excited state, phenols do not undergo excited-state proton transfer in neutral aqueous solution (Laws et al., 1986). Apparently the rate of deprotonation is too slow in water to compete with other decay pathways, but it does become competitive in the presence of high concentrations of proton acceptor (Rayner et al., 1978).

Excited-state proton transfer involving the 8-hydroxyl group is not an important deactivation process in tomaymycin. The ground- and excited-state pKs are about the same, methyl

substitution of the phenolic proton hardly affects the quantum yield of either free or bound drug (Barkley et al., 1986), and high buffer base concentrations (0.5 M phosphate) do not quench the fluorescence. Indirect evidence also argues that intersystem crossing is not a major decay channel. Intersystem crossing rates are generally taken to be independent of temperature. Fluorescence quantum yield data for the DNA adducts can be fit to an Arrhenius equation assuming that the only temperature-independent term is the radiative rate. Iodide and cesium presumably quench fluorescence by enhancing the intersystem crossing rate through the heavy atom effect. They are poor quenchers of tomaymycin fluorescence, though they quench tyrosine fluorescence with moderate efficiency (Homer & Allsopp, 1976).

The molecular modeling studies of 6-mer duplex adducts show substantial shielding of the antibiotic in the minor groove, regardless of the stereochemistry of the covalent linkage or the orientation on the helix. This concurs with fluorescence-quenching data, which indicate a large reduction in the accessibility of the chromophore to acrylamide in the DNA adducts. Only the 5-carbonyl consistently forms H-bonds with the solvent (Table VI). Although the 8-hydroxyl group points away from the DNA core, it prefers an intramolecular H-bond with O7 to intermolecular H-bonds with water except in the S3′ adduct. There is little steric hindrance to replacing the hydroxyl group with a methoxyl group, as seen by nearly identical conformations of tomaymycin– and 8-*O*-methyltomaymycin–d(ATGCAT)$_2$ adducts. Tomaymycin and 8-*O*-methyltomaymycin have about the same biological potency and sequence preferences (Hurley et al., 1988). Even substitution of the bulkier benzyloxy group at the 8-position results in only minor loss of potency and small changes in sequence preference. Together these observations suggest that tomaymycin and 8-*O*-methyltomaymycin adducts might have similar net binding enthalpies. However, the differences of 5–10 kcal/mol obtained in both vacuum (Table III) and solvation (Table V) calculations are significant. Based on net binding enthalpies, the vacuum-simulated interaction of tomaymycin with DNA is favored over the 8-*O*-methyltomaymycin interaction by at least 6 kcal/mol for the two S adducts and the R5′ adduct. The solvent-simulated tomaymycin interaction is favored by 3–5 kcal/mol for the S adducts, whereas the 8-*O*-methyltomaymycin interaction is favored by 7–10 kcal/mol for the R adducts. Here net binding enthalpies are compared instead of total intermolecular interaction energies, because the distortions required for DNA binding are important factors. There is a price in distortion enthalpy to be paid for a good intermolecular interaction. Previously we argued that the major calf thymus DNA adduct for both tomaymycin and 8-*O*-methyltomaymycin is the 11S diastereomer (Barkley et al., 1986). If so, the molecular modeling results support the greater apparent bonding of tomaymycin compared to 8-*O*-methyltomaymycin.

The p*K* of the 8-phenolic proton of tomaymycin is 8.0, and the phenolate anion is essentially nonfluorescent. However, the fluorescence intensity of the tomaymycin–DNA adduct did not decrease until pH >10.5. The 8-*O*-methyltomaymycin–DNA adduct also showed a drop in fluorescence at the same pH. Absorbance measurements at 260 nm revealed that the DNA had undergone a pH-induced helix-to-coil transition. Because it happens with both antibiotics, removal of the phenolic proton alone cannot be responsible for the low intensity at high pH (Figure 7). However deprotonation of N10 could explain an intensity drop in the two adducts. According to the modeling studies the N10 proton of the antibiotic is hydrogen bonded to DNA and would only be exposed upon disruption of the helix. Whatever the reason for the fluorescence decrease at high pH, the 8-hydroxyl group of tomaymycin is stabilized on bonding to DNA and is not titrated at least until pH 10.5. This is probably caused by a change in p*K* due to the negative field of the phosphates (Allison et al., 1981). Jones and Wilson (1981) reported that the p*K* of 3,8-diamino-6-phenylphenanthridine increases by 2.2 units on binding to DNA at 0.12 M Na^+.

Previous molecular mechanics calculations on tomaymycin bonded to d(ATGCAT)$_2$ gave the perferred order of net binding enthalpies in a vacuum for the four binding modes as R5′ > S3′ > S5′ > R3′ (Cheatham et al., 1988). This differs from the order S5′ > R5′ > S3′ ≫ R3′ obtained here (Table III). The only difference between the two calculations was the force field: AMBER 2.0 vs AMBER 3.0, which has some new parameters. Minimized structures from the prior study were used as the starting point in the present study. Therefore, the enthalpy differences cannot come from docking, which might lead to different local minima. Furthermore, the final minimized structures from the two studies were nearly superimposable. It is well known that geometries are relatively insensitive to the force field in molecular mechanics calculations, whereas enthalpies may vary significantly. We have more confidence in the results of the present study because the new parameters in AMBER 3.0 provide better fits to experimentally determined properties of nucleic acids (Singh et al., 1986). Besides the improved force field, the new calculations were further supported by belly dynamics to help avoid local minima. The reliability of nucleic acid models without solvent and counterions is questionable, so we also did calculations including them. The presence of water and counterions did not change the preferred order of binding modes for the tomaymycin adducts (Table V).

The relative stability of different binding modes of the DNA adduct is governed by the free energy change upon adduct formation. Molecular mechanics calculations predict the enthalpic contribution to the free energy. If the entropy change is the same for all four binding modes, then the relative binding enthalpies determine the relative stabilities. Three factors are thought to contribute to entropy changes of DNA–ligand interactions: configurational entropy, counterions, and hydration. The first two of these are probably about the same for the four binding modes. Tomaymycin almost completely fills the DNA minor groove. It is anchored to the floor of the groove by the covalent linkage at C11 and the hydrogen bond at N10, leaving little opportunity for movement within the groove. Also, it bonds to DNA as the neutral species without significant distortion of the helix. Thus, we do not expect much difference between binding modes in configurational entropy or number of counterions condensed on the DNA. This leaves the more elusive entropy change due to hydration.

The modeling studies provide a qualitative picture of the change in ordered (hydrogen-bonded) water accompanying formation of the various DNA adducts. Tomaymycin loses six H-bonds with water involving HO8, HN10, HO11, O8, and O11. The H-bond to O5 is retained, and, in adducts with 5′ orientation, a second H-bond to O5 is formed (Table VI). The intramolecular H-bond between HO8 and O7 remains in all cases except the S3′ adduct, which replaces it with an H-bond to water. New H-bonds to water are formed with O7 in the S adducts and with O8 in the S5′ adduct. The net change in water molecules hydrogen bonded to tomaymycin is therefore a loss of 3–6 in the order S5′ < S3′ < R5′ < R3′. Five waters (356, 362, 394, 568, and 691) are displaced from

the minor groove of $d(ATGCAT)_2$ in adducts with 3′ orientation compared to only three waters (394, 568, and 691) in the 5′ orientation. Thus, formation of a tomaymycin–DNA adduct is accompanied by loss of 6–11 hydrogen-bonded water molecules. A total of three more water molecules are released when tomaymycin is bonded in the 3′ orientation than in the 5′ orientation, suggesting that the 3′ orientation is entropically favored.

References

Allison, S. A., Herr, J. C., & Schurr, J. M. (1981) *Biopolymers 20*, 469–488.

Andre, J. C., Niclause, M., & Ware, W. R. (1978) *Chem. Phys. 28*, 371–377.

Arima, K., Kohsaka, M., Tamura, G., Imanaka, H., & Sakai, H. (1972) *J. Antibiot. 25*, 437–444.

Arnott, S., Campbell, P., & Chandrasekharan, R. (1976) in *Handbook of Biochemistry and Molecular Biology* (Fasman, G., Ed.) CRC Press, Cleveland, OH.

Arora, S. K. (1981) *J. Antibiot. 34*, 462–464.

Barkley, M. D., Cheatham, S., Thurston, D. E., & Hurley, L. H. (1986) *Biochemistry 25*, 3021–3031.

Barkley, M. D., Chowdhury, F. N., & Maskos, K. (1991) *Biochemistry* (submitted).

Bishai, F., Kuntz, E., & Augenstein, L. (1967) *Biochim. Biophys. Acta 140*, 381–394.

Boyd, F. L., Stewart, D., Remers, W. A., Barkley, M. D., & Hurley, L. H. (1990a) *Biochemistry 29*, 2387–2403.

Boyd, F. L., Cheatham, S. F., Remers, W., Hill, G. C., & Hurley, L. H. (1990b) *J. Am. Chem. Soc. 112*, 3279–3289.

Cheatham, S., Kook, A., Hurley, L. H., Barkley, M. D., & Remers, W. (1988) *J. Med. Chem. 31*, 583–590.

Creed, D. (1984) *Photochem. Photobiol. 39*, 563–575.

Eftink, M. R., & Ghiron, C. A. (1976) *J. Phys. Chem. 80*, 486–493.

Eftink, M. R., & Ghiron, C. A. (1981) *Anal. Biochem. 114*, 199–227.

Ferrin, T. E., Huang, C. C., Jarvis, L. E., & Langridge, R. (1988a) *J. Mol. Graphics 6*, 1–12.

Ferrin, T. E., Huang, C. C., Jarvis, L. E., & Langridge, R. (1988b) *J. Mol. Graphics 6*, 13–27.

Gally, J. A., & Edelman, G. M. (1962) *Biochim. Biophys. Acta 60*, 499–509.

Graves, D. E., Pattaroni, C., Krishnan, B. S., Ostrander, J. M., Hurley, L. H., & Krugh, T. R. (1984) *J. Biol. Chem. 259*, 8202–8209.

Graves, D. E., Stone, M. P., & Krugh, T. R. (1985) *Biochemistry 24*, 7573–7581.

Hertzberg, R. P., Hecht, S. M., Reynolds, V. L., Molineux, I. J., & Hurley, L. H. (1986) *Biochemistry 25*, 1249–1258.

Homer, R. B., & Allsopp, S. R. (1976) *Biochim. Biophys. Acta 434*, 297–310.

Hurley, L. H. (1977) *J. Antibiot. 30*, 349–370.

Hurley, L. H., & Needham-VanDevanter, D. R. (1986) *Acc. Chem. Res. 19*, 230–237.

Hurley, L. H., Gairola, C., & Zmijewski, M. (1977) *Biochim. Biophys. Acta 475*, 521–535.

Hurley, L. H., Reck, T., Thurston, D. E., Langley, D. R., Holden, K. G., Hertzberg, R. P., Hoover, J. R. E., Gallagher, G., Jr., Faucette, L. F., Mong, S.-M., & Johnson, R. K. (1988) *Chem. Res. Toxicol. 1*, 258–268.

Jones, R. L., & Wilson, W. D. (1981) *Biopolymers 20*, 141–154.

Jorgensen, W., Chandresekhar, T., & Madura, T. (1983) *J. Chem. Phys. 79*, 926–935.

Kirby, E. P., & Steiner, R. F. (1970) *J. Phys. Chem. 74*, 4480–4490.

Kohn, K. W., & Spears, C. L. (1970) *J. Mol. Biol. 51*, 551–572.

Kohn, K. W., Glaubiger, D., & Spears, C. L. (1974) *Biochim. Biophys. Acta 361*, 288–302.

Laws, W. R., Ross, J. B. A., Wyssbrod, H. R., Beechem, J. M., Brand, L., & Sutherland, J. C. (1986) *Biochemistry 25*, 599–607.

Löber, G. (1981) *J. Lumin. 22*, 221–265.

Maruyama, I. N., Tanaka, N., Kondo, S., & Umezawa, H. (1979) *J. Antibiot. 32*, 928–934.

Marzilli, L. G. (1976) *Prog. Inorg. Chem. 23*, 255–378.

Melhuish, W. H. (1961) *J. Phys. Chem. 65*, 229–235.

Nishioka, Y., Beppu, T., Kohsaka, M., & Arima, K. (1972) *J. Antibiot. 25*, 660–667.

Norman, D., Live, D., Sastry, M., Lipman, R., Hingerty, B. E., Tomasz, M., Broyde, S., & Patel, D. J. (1990) *Biochemistry 29*, 2861–2875.

Olmsted, J., III, & Kearns, D. R. (1977) *Biochemistry 16*, 3647–3654.

Prive, G. G., Heinimann, U., Chandrasegaran, S., Kan, L.-S., Kopka, M. L., & Dickerson, R. E. (1987) *Science 238*, 498–504.

Rayner, D. M., Krajcarski, D. T., & Szabo, A. G. (1978) *Can. J. Chem. 56*, 1238–1245.

Remers, W. A., Mabilia, M., & Hopfinger, A. J. (1986) *J Med. Chem. 29*, 2492–2503.

Seibel, G. L., Singh, U. C., & Kollman, P. A. (1985) *Proc. Natl. Acad. Sci. U.S.A. 82*, 6537–6540.

Singh, U. C., & Kollman, P. A. (1984) *J. Comput. Chem. 5*, 129–145.

Singh, U. C., Weiner, P. K., Caldwell, J., & Kollman, P. A. (1986) AMBER (UCSF) version 3.0, Dept. of Pharmaceutical Chemistry, University of California, San Francisco.

Sur, A., & Johnson, P. M. (1986) *J. Chem. Phys. 84*, 1206–1209.

Weiner, S. J., Kollman, P. A., Case, D. A., Singh, U. C., Ghio, C., Alagona, G., Profeta, S., Jr., & Weiner, P. (1984) *J. Am. Chem. Soc. 106*, 765–784.